Before the breach: Interactions between colloidal particles and liquid interfaces at nanoscale separations

Anna Wang, Jos W. Zwanikken, David M. Kaz, Ryan McGorty, Aaron M. Goldfain, W. Benjamin Rogers, and Vinothan N. Manoharan

Phys. Rev. E **100**, 042605 — Published 9 October 2019

DOI: 10.1103/PhysRevE.100.042605

Before the breach: Interactions between colloidal particles and liquid interfaces at nanoscale separations

Anna Wang,[1,2] Jos W. Zwanikken,[3] David M. Kaz,[4,5] Ryan McGorty,[4,6]
Aaron M. Goldfain,[1] W. Benjamin Rogers,[1,7] and Vinothan N. Manoharan[1,4]

[1] *Harvard John A. Paulson School of Engineering and Applied Sciences, Harvard University, Cambridge MA 02138 USA*
[2] *School of Chemistry, UNSW Sydney, Kensington NSW 2052 Australia*
[3] *Department of Physics, University of Massachusetts, Lowell MA 01854 USA*
[4] *Department of Physics, Harvard University, Cambridge MA 02138 USA*
[5] *Present address: Agilent Technologies, Santa Clara, CA 95051*
[6] *Department of Physics and Biophysics, University of San Diego, San Diego CA 92110*
[7] *Martin Fisher School of Physics, Brandeis University, Waltham MA 02453 USA*

Particles bound to fluid-fluid interfaces are widely used to study self-assembly and to make materials such as Pickering emulsions. In both contexts, the lateral interactions between such particles have been studied extensively. However, much less is known about the normal interactions between a particle and the interface prior to contact. We use digital holographic microscopy to measure the dynamics of individual, micrometer-sized colloidal particles as they approach an interface between an aqueous phase and oil. Our measurements show that the interaction between the particle and interface changes nonmonotonically as a function of salt concentration, from repulsive at 1 mM to attractive at tens of mM to negligible at 100 mM and attractive again above 200 mM. In the attractive regimes, the particles can bind to the interface at nanometer-scale separation without breaching it. Classical DLVO theory does not explain these observations. However, a theory that accounts for non-linear screening and correlations between the ions does predict the non-monotonic dependence on salt concentration and produces trajectories that agree with experimental data. We further show that the normal interactions determine the lateral ones between particles that are bound to the interface. Because the interactions we observe occur at salt concentrations used to make Pickering emulsions and other particle-laden interfaces, our results suggest that particle arrangements at the interface are likely out of equilibrium on experimental time scales.

I. INTRODUCTION

The strong attraction between solid colloidal particles and fluid interfaces has enabled a wide range of practical applications and fundamental condensed-matter studies. This attraction is usually explained by partial wetting: a particle that sticks to the interface in fact breaches it, so that it is partially wetted by both phases. The breaching removes some of the interfacial area, typically yielding a decrease in interfacial energy per particle of 10^2–10^7 times the thermal energy kT [1]. The adsorbed particles can stabilize droplets of one liquid (such as oil) in another, immiscible one (such as water), even in the absence of surfactants [2]. These systems, called Pickering emulsions, are useful for encapsulation [3], biological assays [4], and making nanostructured materials [1, 5, 6]. Similar systems, in which particles adsorb to planar air-water interfaces, are used to create model two-dimensional systems for studying phase transitions [7–9].

Yet even in the simplest systems, which consist of spherical solid particles and planar interfaces—and where the particles are sufficiently small that they do not distort the interface—the interactions between adsorbed particles are surprisingly complex. We call these the *lateral* interactions (Fig. 1A). Experiments have reported lateral interactions that are repulsive and long-ranged [10], attractive and long-ranged [11, 12] and/or heterogeneous [13–15]. These experiments have spurred the development of increasingly sophisticated models of the electrostatic interactions between adsorbed particles [16–18] and have highlighted the role of lateral capillary interactions [12, 19] induced by contact-line pinning. Understanding the lateral interactions is important because they control emergent properties such as the interfacial rheology, stability of Pickering emulsions, and dynamics of self-assembly at the interface.

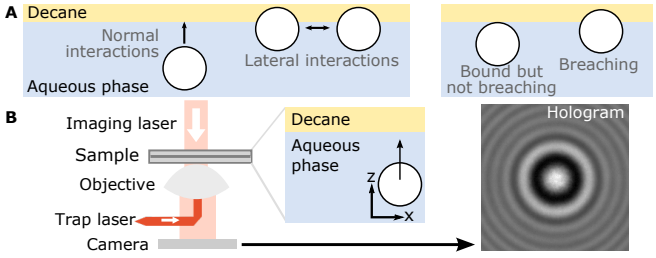

FIG. 1. (A) Left, schematic of the normal and lateral interactions; right, schematic of two ways in which particles can bind to the interface. (B) Diagram of all-optical apparatus used to push a particle to an interface and capture holograms, which are used to measure the particle position in three dimensions.

Less well-studied are the *normal* interactions, which operate between a particle and the interface (Fig. 1A). The normal interactions can determine the lateral interactions; for instance, the electrostatic interactions between particles at the interface depend on how much the particles protrude into either phase. To understand the normal interactions, we measure the dynamics of adsorp-

tion as a function of salt concentration with high spatial and temporal precision. Our experiments reveal the height of the particle relative to the interface [20, 21] and the fluctuations in height with time. By contrast, many previous experiments do not measure these variables, and thus do not reveal whether the particle has reached its equilibrium height or even if it has breached the interface in the first place.

By studying the dynamics in detail, we find that the normal interaction appears to vary nonmonotonically with salt concentration. Using a liquid-state theory of electrostatic interactions, we show that the normal interactions between the particle and the interface and its salt dependence arise from the structure of the ion cloud around the particles, and the geometric constraints imposed by the interface and the colloidal surface. We then illustrate the relevance of our single-particle observations to bulk phase behavior by studying the assembly of particles at an interface. Overall, our observations of the interactions and dynamics, which occur over a range of salt concentrations that are not infrequently used in Pickering-like systems, illustrate the critical role that nonequilibrium processes might play in the self-assembly of particles at interfaces.

II. RESULTS AND DISCUSSION

We use digital holographic microscopy (Fig. 1B) to track colloidal particles with nanometer-scale precision in all three dimensions as they approach a planar oil-water interface, where glycerol is added to the aqueous phase to match the refractive index of the oil (see Appendix A). We push each particle gently toward the interface with radiation pressure from an out-of-focus optical trap [20]. In all of our experiments, the particle remains free to rotate, and the interface remains undeformed under the weak radiation pressure: Given a maximum radiation force of 10^{-12} N and an interfacial tension of 37 mN/m, the deformation of the interface should be less than 0.1 nm. Because our measurements track the particle height over time—even after it breaches the interface—we can distinguish between different modes of binding.

A. Three types of normal interactions

We find that the interaction between the particle and the interface depends on the salt concentration. At 100 mM NaCl and higher, all the trajectories of sulfate- and carboxyl-functionalized polystyrene particles show a kink (Fig. 2A), the signature of partial wetting [20]. After the kink, the particles are so strongly bound to the interface that we cannot remove them with the optical trap. At 25 mM NaCl and lower, the initial part of the trajectories looks similar to that at higher salt concentrations, but there is no kink (Fig. 2B and Fig. 2C). These trajectories suggest that there is a repulsive barrier to breaching

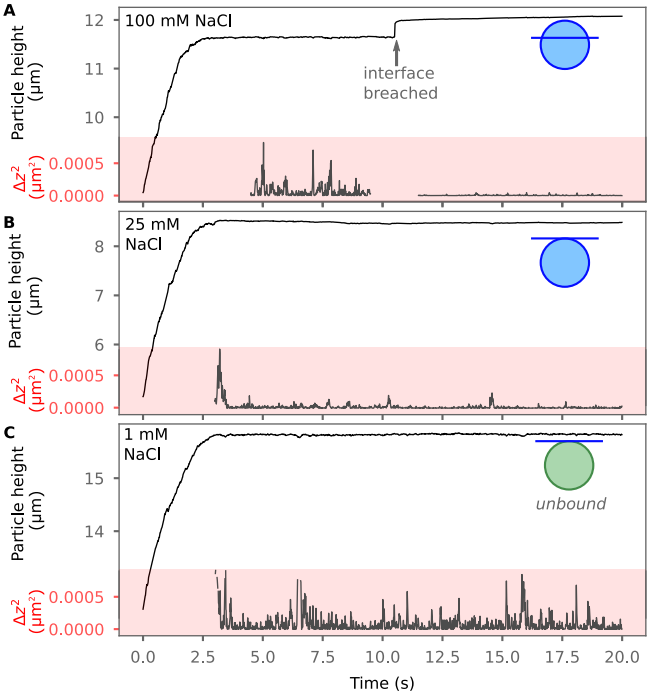

FIG. 2. Negatively-charged polystyrene particles show three types of normal interactions. The upper plots show the height z of 1.9-μm-diameter sulfate polystyrene particles (measured from the focal plane of the objective) as the particles move toward an interface between glycerol/water and decane under weak radiation pressure (data shown at 100 Hz). The lower plots show the fluctuations in height, Δz^2, defined as the square of the particle's displacement from its mean height at a given time t, as calculated from a centered sliding average with a 1 s window. (A) At moderate NaCl concentrations (100 mM), particles breach the interface (11 s). Because of the rapid movement of the particle during the breach, we do not show the fluctuations in this part of the trajectory. (B) At low NaCl concentrations (tens of mM), particles approach the interface and bind to it without breaching it. Binding is evidenced by the decrease in fluctuations at about 4 s. (C) At very low salt concentrations (less than 10 mM), particles approach the interface and do not bind, as evidenced by the large fluctuations.

the interface. Indeed, at salt concentrations of 10 mM NaCl or lower, we can remove the particles with the optical trap, and we cannot force them to adsorb even by applying the maximum upward radiation force of about 10 pN.

However, at salt concentrations of 25 mM, we cannot remove particles from the vicinity of the interface using the optical trap. Furthermore, although the trajectories of particles at 25 mM NaCl (Fig. 2B) appear almost identical to those at 1 mM (Fig. 2C)—that is, there is no kink, and the raw trajectories agree well with those predicted by hydrodynamic calculations [20, 22]—the fluctuations in particle height (lower plot of Fig. 2B) are comparable to those of a particle that has breached the interface (lower plot of Fig. 2A) and much smaller than those of

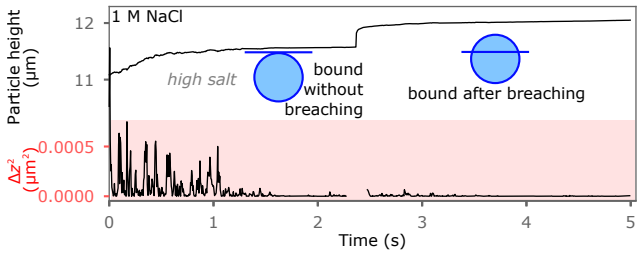

FIG. 3. Binding without breaching also affects particles at high salt concentrations before they breach. Top plot shows a 200-Hz trajectory of a 1.4-μm-diameter particle in a 1 M NaCl aqueous solution. The reduction in fluctuations from the mean position averaged over a 0.2 s window (bottom plot) reveals that the particle binds to the interface at about 1.5 s without breaching it. The particle breaches the interface at around 2.5 s.

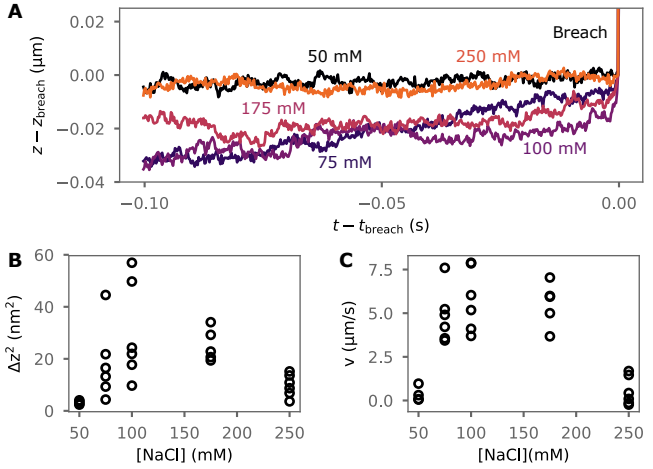

FIG. 4. Binding without breaching is reentrant with salt concentration. The trajectories (A) are of 2.0-μm-diameter carboxyl latex particles and are taken at 4807.7 Hz. z_{breach} is the height of the particle in the frame just before the breach, which occurs at t_{breach}. The fluctuations (B, left) are calculated from a centered 0.2 s sliding average of $z(t)$; the speed of the particle (B, right) $\Delta z/\Delta t$ is measured at $\Delta t = 2.08$ ms before the breach. The particles at the highest and lowest salt concentrations breach abruptly and have smaller fluctuations before breaching. Particles at intermediate concentrations have larger fluctuations and speeds before breaching.

particles at low salt concentration (lower plot of Fig. 2C). Both of these observations indicate that the particles are caught in a potential well.

The measured fluctuations also reveal that a potential well affects particles at NaCl concentrations much greater than 100 mM NaCl, though at these concentrations all particles eventually breach. The 1.4-μm-diameter sulfate latex particle shown in Fig. 3 is in a 1 M NaCl solution and binds to the interface without breaching for about 1 s before it finally breaches. The presence of binding without breaching at high salt concentrations, where electrostatic interactions are heavily screened and particles should breach readily, is surprising.

Taken together, these observations show that there are three different normal interactions in four salt regimes: At very low salt (10 mM or lower), no breaching occurs, and the particle is repelled by the interface. At low salt (tens of mM), particles bind to the interface without breaching it. At moderate salt (100 mM), particles bind to the interface only through a capillary interaction (they do not bind before breaching). At high salt (greater than 100 mM), particles bind to the interface without breaching and subsequently breach.

High-speed measurements of the trajectories and fluctuations for 2.0-μm-diameter carboxyl latex particles confirm that the attraction between the particle and interface is non-monotonic with salt concentration (Fig. 4). Particles at low (50 mM) and high (250 mM) NaCl concentrations breach abruptly, whereas particles at moderate concentrations (75–175 mM) accelerate toward the interface before breaching it (Fig. 4A). The small fluctuations of the particles at 50 mM and 250 mM NaCl (Fig. 4B) show that they are in an attractive well before breaching. By contrast, the particles at salt concentrations between these values breach from an unbound state (Fig. 4C).

We find also that the normal interactions can vary with time. For example, at low NaCl concentrations (50 mM and below), we observe both polystyrene and silica particles (see Appendix C) bind, unbind, then bind again in less than a minute. Our observations of reentrant attraction and variation with time suggest that the electrostatic interactions are more complex than simple double-layer interactions, which we would expect to vary monotonically with salt concentration.

B. Lateral interactions

Because we expect the lateral interaction between particles to control the properties of particle-laden interfaces such as Pickering emulsions, we also explore such interactions between both types of bound particles—those that have breached and those that have not. We suspend 1.9-μm-diameter sulfate polystyrene particles in various NaCl concentrations from 25 to 100 mM without any glycerol. We invert the sample cells to allow particles to sediment toward the oil-water interface for 1 h, then turn them back upright and image the interface after 1 h, allowing any unbound particles to settle after the sample is turned upright. All particles are therefore either bound to the interface (whether breaching or not) or at the bottom of the sample chamber; none remain suspended. Furthermore, the interface is not saturated with particles in any of the samples.

We find that the fraction of particles that bind to the interface increases with the salt concentration, as expected from our holographic measurements of the normal interactions. By comparing microscopy images of the bottom of the sample chamber (see Appendix C) to

those of the interface, we find that at 25 mM (Debye screening length $\kappa^{-1} \approx 1.9$ nm), about 35% of particles bind, while at 37.5 mM ($\kappa^{-1} \approx 1.6$ nm) about 95% bind. At salt concentrations from 50 to 100 mM, the particles form long-ranged repulsive crystals, similar to those reported in other studies [7, 10]. We note that in the glycerol-free system shown here, the critical salt concentration at which all particles breach is 50 mM. For the glycerol/water system used in the holography experiments, the critical concentration is 100 mM.

Although the interfaces at lower salt concentrations appear disordered (Fig. 5), some of the particles are in fact ordered. Because breaching particles are partially wetted by decane, we can distinguish them optically from those that do not breach the interface: breaching particles have a lower relative refractive index ($m_{\text{decane}} = n_{\text{particle}}/n_{\text{decane}} = 1.12$) and have lower contrast than particles that are bound without breaching ($m_{\text{water}} = 1.19$). Identifying only the breaching particles, as shown in Fig. 5B, makes it clear that they form a repulsive crystal. The apparent disorder at the interface is due to the presence of particles that are bound without having breached (Fig. 5C). Although we do see a weak attraction between particles bound without breaching and those that have breached (see Appendix E, Movie 1), this attraction does not appear to affect the formation of the repulsive crystal.

Once the particles that are bound without breaching eventually breach, they force the breaching particles to rearrange. Thus, the number of breaching particles and the ordering of particles at the interface increases with time, as shown in Fig. 6. The order is evidenced by the distinct peaks in the Fourier transforms of the micrographs. At longer times, the Fourier peaks become brighter, and the spacing between peaks increases, reflecting a decrease in the lattice spacing (Fig. 6B–C).

From these observations we conclude the following. There are two types of bound particles—particles that breach the interface and particles that are bound without breaching—and three types of lateral interactions: (1) Breaching particles interact with other breaching particles through a strong repulsive interaction that causes them to crystallize; (2) bound-but-not-breaching particles interact weakly with other bound-but-not-breaching particles; and (3) bound-but-not-breaching particles have a weak attraction to breaching particles. Thus, the normal interaction (binding by breaching or binding without breaching) determines the lateral interactions at the interface.

Finally, we consider what our observations tell us about many-particle effects. The fact that the bound-but-not-breaching particles do not perturb the crystal formed by the breaching particles suggests that interactions of type (3) do not affect interactions of type (1).

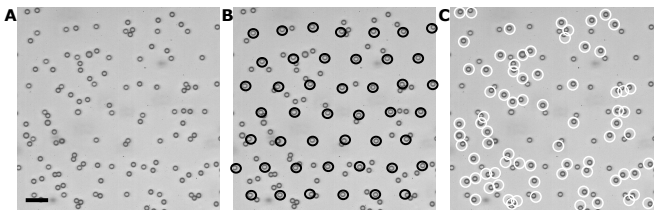

FIG. 5. Lateral interactions between particles breaching the interface appear unaffected by those that have bound without breaching. Panels show the same optical micrograph of particles at or near the interface in a sample with 37.5 mM salt. In (B), breaching particles are circled, showing that these particles have formed a crystal. The ordering is not readily apparent in (A). In (C), the particles that have bound without breaching are circled. Scale bar represents 10 μm.

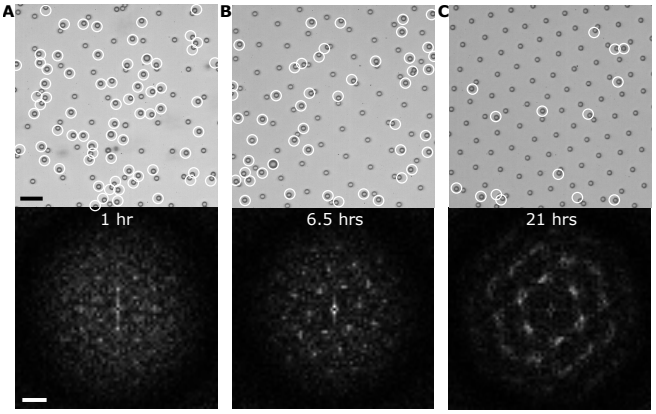

FIG. 6. The interface becomes more ordered over time, as particles that are bound without breaching eventually breach and become part of the crystal. Top row shows bright-field microscopy images of a 37.5 mM NaCl sample at (A) 1 h, (B) 6.5 h, and (C) 21 h after the sample is inverted. Particles that are bound without breaching are circled. Bottom row shows Fourier transforms of the top images, with the central DC pixel blocked to enhance contrast. Scale bars are 10 μm (top) and 0.1 μm^{-1} (bottom).

C. Characterizing the normal interaction

The results of the previous section show that the structure of particles at an interface is determined not only by particles that bind by breaching, but also by particles that bind without breaching. Therefore, we now turn to understanding the origins of binding without breaching.

Jensenius and Zocchi [23] found that polystyrene spheres have surface-bound polymer chains, approximately 50 nm long, that can tether the particles to a surface with an effective stiffness of 1.5 mN/m. Such tethering is unlikely to be responsible for the interactions we observe, for two reasons. First, we observe a similar attraction with silica particles (see Appendix C), which should not have any surface-bound chains. Second, the attraction is reentrant with salt concentration. Although reentrant effects have been reported in polymers, they appear to result from strong electrostatic interactions in multivalent salt solutions [24, 25], conditions dif-

ferent from those in our system.

Leunissen and coworkers [26] and Kelleher and coworkers [27] showed that colloidal particles in oil can bind to an oil-water interface without wetting the aqueous phase. The attraction arises from image-charge attraction, extreme hydrophobicity, and, as shown recently, repulsive van der Waals forces [28]. However, in this system, the state in which particles bind without breaching is the lowest-energy state. In ours, particles that are bound without breaching can reach a lower-energy state by breaching. Furthermore, in our system, the particles are in the aqueous phase, and the image-charge forces are repulsive, not attractive. Finally, we observe a more complex set of interactions as a function of the salt concentration.

The short-ranged, secondary minimum predicted by Derjaguin, Landau, Verwey, and Overbeek theory (DLVO) at certain salt concentrations [29] might seem to explain the interaction we see. Helden, Dietrich, and Bechinger [30] used DLVO theory to fit experimental measurements of the interaction between oil droplets and an oil-water interface. However, for our experimental system, DLVO does not explain the observed binding, nor does it account for its re-entrance at higher salt concentrations (see Appendix D). In our system, the van der Waals interaction between a particle and the interface is much weaker than in the system used by Helden, Dietrich, and Bechinger, where the oil phase had a refractive index of 1.47.

Having determined that none of the above non-electrostatic and classical electrostatic arguments explain our observations of the binding, we turn to a more sophisticated electrostatic model based on a liquid-state theory [31–33]. The theory accounts for the effect of electrostatic screening by the ions, similar to widely used theories such as DLVO and Poisson-Boltzmann/Gouy-Chapman, but it treats the ions as finite-sized particles instead of as a structureless cloud of point particles. Classical DLVO theory does not account for the non-linear screening and the steric effects, which we expect to be important at the salt concentrations used in the experiments, based on the predictions of Zwanikken and coworkers [31] and Jing and coworkers [33]. For these concentrations it was found that correlations have a significant effect on the ion density and the osmotic pressure, close to an interface, if the salt concentration exceeds about 100 mM. We calculate the activity coefficient of the ions, via the pair correlation functions, by solving the Ornstein-Zernike (OZ) equation under the Anisotropic Hypernetted-Chain closure (AHNC), based on the initial work of Kjellander and Marčelja [32]. The ions are assumed to be hard, unpolarizable spheres with a diameter of 0.7 nm (larger than the Bohr radius due to hydration) with a Coulomb potential. For further details see Appendix B.

We find that monovalent ions at concentrations above 100 mM show a distinct structure resembling that of a correlated liquid rather than a gas of point particles or a frozen solid, as in the work by Zwanikken and coworkers [31] and Jing and coworkers [33]. Because of the boundary conditions imposed by the oil-water interface and the colloidal surface, the ions do not form the lowest-energy structure that they would form in bulk, but instead form a compromised structure, leading to a slightly positive contribution to the chemical potential near the particle and the interface. Although the effect is small for a single ion—the chemical potential of a single confined ion increases by a fraction of the thermal energy—the contribution by the affected ion cloud of a colloidal particle can easily exceed the thermal energy. After calculating the pair correlation functions and the position-dependent chemical potential of the ions using OZ-AHNC theory, we evaluate the local density according to the (non-ideal) Boltzmann distribution and, finally, the osmotic disjoining pressure between the colloidal surface and the water-decane interface by summing all the forces that the confined ions exert on the boundaries [31–33]. This approach also explicitly includes the effects of polarization charge at the interface and the colloidal surface. Dispersion forces are included similarly to DLVO theory, after estimating an appropriate Hamaker constant. The method involves very few assumptions in the statistics apart from the (highly accurate) AHNC closure, but it does include simplifying assumptions: the liquids are assumed to be uniform structureless dielectric media, the colloidal surface perfectly flat, and the ion cloud in an equilibrium state.

Using this approach with parameters corresponding to our experimental system, we find two regimes in which particles bind without breaching. For 1.9-μm-diameter sulfate polystyrene beads near an interface between glycerol/water and decane, there is a potential well about 1–12 nm from the interface for NaCl concentrations between 20 and 70 mM (Fig. 7), consistent with our observations (Fig. 4). At salt concentrations above 325 mM NaCl, the simulations again predict a potential well, at a slightly higher salt concentration than that observed in experiments (250 mM).

The potential well at lower salt concentrations arises from the competition between a van der Waals attraction and a screened Coulomb repulsion, reminiscent of DLVO but including important additional effects that become dominant at higher salt concentrations, as mentioned above. Our calculations show that the screened Coulomb interaction collapses upon addition of salt much more drastically than in DLVO, and even becomes attractive above approximately 100 mM.

At higher salt concentrations (325–350 mM), the screened Coulomb potential develops oscillations, including a potential barrier near contact. These effects originate from the structure in the ion cloud and the geometric constraints that the oil-water interface and the colloidal particles impose on the structure. The oscillations in the landscape of the effective potential result from a balance between optimal packing and an optimal electrostatic configuration.

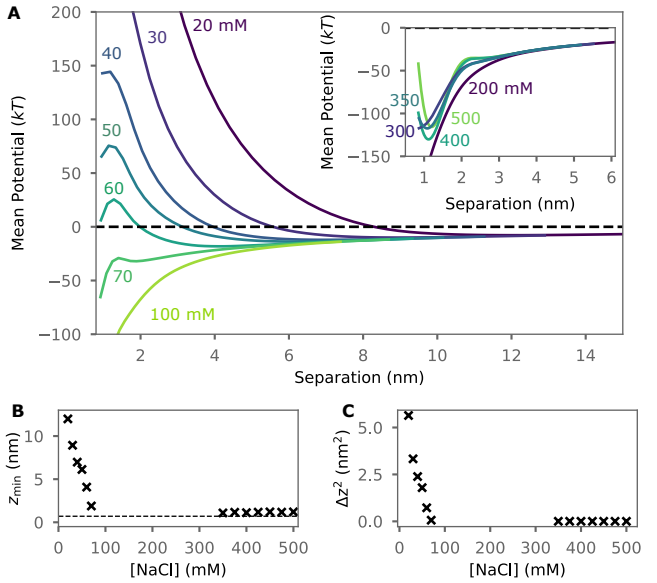

FIG. 7. A liquid-state theory predicts mean potentials between a polystyrene particle and an interface with glycerol/water on one side and decane on the other. The calculations reveal a potential well at 20–70 mM NaCl and above 325 mM NaCl (inset). B. The position of the potential minimum $z_{\min}$ decreases with increasing salt concentration, disappears, then reappears at higher salt concentration. The ion diameter is shown by the dotted line. C. The fluctuations of the particle in the well also decrease with salt concentration until the well disappears at about 70 mM. At concentrations above 325 mM, the well appears again.

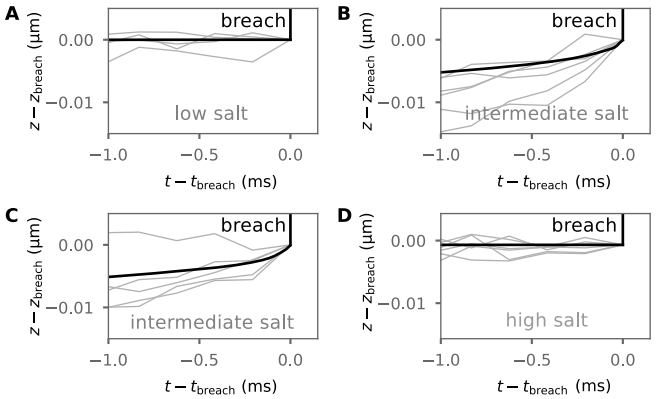

FIG. 8. Trajectories of particles prior to breaching agree with model predictions. Measured trajectories are shown in gray and trajectories calculated from our model in black. A. At low salt concentration (50 mM), particles bind to the interface before breaching. B. At moderate salt concentrations (100 mM), particles breach the interface without binding first. Furthermore, they accelerate toward the interface before breaching. C. Similar behavior as in B but for 175 mM NaCl in experiment and 200 mM in calculations. At high salt concentrations (250 mM NaCl in experiment and 350 mM NaCl in calculations), particles bind to the interface before breaching, and no acceleration is seen.

The discrepancy between the observed (250 mM) and predicted (325–350 mM) salt concentrations at which the potential well re-enters is not surprising, given that at high salt concentrations, the calculations are sensitive to parameters such as the Hamaker constant and charge of the particles. Indeed, our observations of time-varying interactions (Fig. 6, Fig. 9, and Fig. 10) suggest that the particle charge density is not homogeneous. Kang, Lim, and Park [34] came to the same conclusion for a similar system. We hypothesize that the variations in the interactions with the interface could be due to rotational diffusion: as the particle rotates, patches with varying amounts of charge are presented to the interface, changing the close-range electrostatic interaction of the particle with the interface. In our model, we assume that the surface charge of the particles is homogeneous.

Importantly, the model predicts the re-emergence of a regime where particles can bind without breaching at higher salt concentrations, which is consistent with our experimental observations and not predicted by DLVO theory. Because the strength of the interaction is many times the thermal energy, the particle can remain bound for minutes or hours before breaching, in agreement with our observations at moderate salt concentrations.

Furthermore, the expected fluctuations of the particle in the potential well and the location of the well are of the correct order of magnitude at both low and high salt, where we consider the high salt condition to be 250 mM in experiment and 350 mM in the model. Low salt corresponds to 50 mM in both cases. The measured fluctuations (Δz^2; see Appendix D) of particles that are bound to the interface are less than 4 nm^2 at both low and high salt, where 4 nm^2 is the noise floor of our instrument. The predictions from the model are 1–6 nm^2 at low salt and 1 nm^2 at high salt. We estimate the location of the particle relative to the interface ($z_{\min}$) from the maximum displacement of the particle over 10 ms, as observed in the experiments in Figure 4A. We find $z_{\min} <$ 10 nm at both low and high salt, in agreement with the predicted $z_{\min}$ of 1–12 nm at low salt and 1 nm at high salt.

A more stringent test of our model is whether it produces particle trajectories that agree with the observed ones. To calculate the trajectories from the model, we assume a shear free boundary [20] and equate the drag force [22] with the force $F(z)$ between the particle and the interface as predicted by our model plus the upward radiation force from the optical trap $F_{\mathrm{r}} = 0.3$ pN (estimated from the velocities of particles in Fig. 2) and the buoyant force F_{b}:

$$F(z) + F_{\mathrm{r}} + F_{\mathrm{b}} = F_{\mathrm{d}} = 6\pi\eta R v, \qquad (1)$$

where η is the viscosity of the aqueous solution (9.39 mPa·s [35]), R is the particle radius, and v the particle velocity. We then numerically integrate over 1 ms prior to the breach. The resulting trajectories agree well with the measured ones after we rescale the salt concentrations such that high salt corresponds to 250 mM

in experiment and 350 mM in calculations (see Fig. 8). Importantly, the model captures the acceleration of particles toward the interface at salt concentrations where particles breach without binding. The shapes of the calculated trajectories also agree with experiment to within the uncertainty of the experimental data, as illustrated by the different measured trajectories shown in Fig. 8.

D. Implications

There are several possible reasons for the absence of earlier reports on the normal interactions we observe. In AFM experiments, the applied forces are large enough to deform the interface [36], and the particles are immobilized on the cantilever tip, which artificially constrains their motion. In optical microscopy experiments, it is difficult to distinguish particles that have breached the interface from those that lie just below it—unless one knows that there are two different binding modes. Indeed, the two binding modes cannot be distinguished by analyzing fluctuations (see Appendix D); thus, determining the binding mode requires tracking the particles before they breach. Finally, most experiments on particles at interfaces use a spreading solvent to deposit particles at the interface, which creates a mixing layer and prevents the particle from interacting with the pure oil-water interface.

Nonetheless, Pickering emulsions and many other interfaces containing particles are prepared without spreading solvents, and the normal interactions we observe could be critical for understanding the behavior of such systems. As Wang, Singh, and Behrens [37] noted, it is useful to add salt when preparing particle-laden interfaces from particles that are dispersed in the aqueous phase, because the salt reduces the electrostatic barrier to breaching posed by image-charge repulsion. Reducing the barrier increases the fraction of particles that can bind to the interface. However, it is precisely under these conditions (moderate to high salt concentration) that we observe particles bind without breaching the interface. Microscopic observations of such interfaces might not reveal the true picture of how the particles are arranged. As we have shown, seemingly disordered interfaces might actually contain a mixture of disorder and order, with the breaching particles forming the ordered array.

Our experiments also show that it can take a long time (hours to days) for particles that are bound to eventually breach. This observation, along with recent findings that particles can take days to months to reach their equilibrium contact angle once they do breach, owing to contact-line pinning [20, 21], shows that particle-laden interfaces can easily be out of equilibrium on experimental time scales. Therefore, models of lateral interactions that assume equilibrium might not be able to explain the structure or dynamics of particle-laden interfaces, including those of Pickering emulsions.

The effects of the normal interactions on the stability of Pickering emulsions are worthy of future study. At high particle concentrations, the interface might at first be crowded with bound (but not breaching) particles, owing to their weak lateral interactions. But if the breached particles are the ones that confer stability, it is their surface concentration that matters. That surface concentration may saturate as particles that are bound without breaching eventually breach, and their lateral interactions become repulsive and long-ranged.

The agreement between our experimental results and the model shows that ion structure is critical to understanding the interactions between the particle and interface. Heterogeneity in the charge of the particle or interface (or both) also appears to be an important feature at such small separations. Overall, our results show that these electrostatic effects make the seemingly simple process of breaching—where a particle makes contact with the interface and protrudes through it—into a complex and sometimes rare event. The last few nanometers before the interface can be the most difficult to traverse.

ACKNOWLEDGMENTS

We thank Michael Brenner, Lucio Isa, Madhav Mani, Monica Olvera de la Cruz, Fyl Pincus, Rudi Podgornik, and Jan Vermant for illuminating discussions. This work was funded by the National Science Foundation through grant no. DMR-1306410 and by the Harvard MRSEC through NSF grant no. DMR-1420570. This work was performed in part at the Harvard University Center for Nanoscale Systems (CNS), supported by NSF grant no. 1541959.

Appendix A: Materials and Methods

All materials are carefully cleaned to minimize contamination and maintain a surfactant-free interface. Glassware is cleaned in a pyrolysis oven (Pyro-Clean Tempyrox) then rinsed in deionized water (Milli-Q system, EMD Millipore). Plastic components are sonicated in three changes of methanol, then water, then rinsed in water. We remove the decane ($\geq$ 99% anhydrous, Sigma Aldrich) from the SureSeal bottle with a stainless steel hypodermic needle (Cadence Science) on a glass syringe (Hamilton), and we filter the decane through a 0.2 μm pore-size polytetrafluoroethylene membrane filter (Acrodisc). We store the decane in a borosilicate glass vial (cleaned in the pyrolysis oven) with a teflon-lined lid (Wheaton) and reserve some decane in a separate clean glass vial for rinsing the syringe and needle prior to taking future aliquots of decane. We measure the interfacial tension between glycerol/water and decane by ring tensiometry and find that it is 37 mN/m. We also measure the interfacial tension using the pendant-drop method. To be able to see the drop, we introduce a slight refractive-index mismatch between the oil and aqueous phases by

using 61% (w/w) glycerol for the aqueous phase. We find that the interfacial tension is 37 ± 2 mN/m (n = 11 measurements). The measured interfacial tension is consistent with the interface being free from contamination [38].

We suspend colloidal particles in aqueous solutions with 1.0 mM to 1 M NaCl. In holographic imaging experiments, glycerol (59% w/w) is added to match the refractive index of the aqueous phase to that of the oil, decane (n = 1.411). The index-matching eliminates reflections from the oil-water interface and maximizes the precision of our holographic measurements. A small volume (2–4 μL) of each suspension and a bath of filtered decane are added to a custom sample cell [20], and the two liquids are allowed to equilibrate for at least 30 minutes.

The particles are 1.4- and 1.9-μm-diameter sulfate-functionalized polystyrene particles (Invitrogen), and 2.0-μm-diameter carboxyl-functionalized polystyrene particles (Invitrogen). We also silanize some 1-μm-diameter silica spheres (Bangs Laboratories): we suspend 6% w/w particles in 3 mL ethanol, then add 0.1 mL (3-aminopropyl)trimethoxysilane (97% Sigma-Aldrich) and 50 μL 30% ammonium hydroxide solution (30%, JT Baker) and wait for 4 h. We wash all particles by repeated centrifugation and resuspension in deionized water (Milli-Q system, EMD Millipore). For sulfate-polystyrene spheres in water/glyercol at 100 mM NaCl we measure ζ_s = -55 mV (Delsa Nano C, Beckman Coulter).

The sample cells are placed on a Nikon TE-2000 inverted microscope equipped with two counter-propagating lasers, an 830 nm laser used as an optical trap and a 658 nm laser used to generate holograms [20]. Particles in the aqueous suspension are initially placed several micrometers below the liquid interface using the optical trap. The trap is then deactivated, positioned several micrometers below the particle, and reactivated, thus pushing the particle upward with nearly uniform radiation pressure. A high-speed camera (Photon Focus MVD-1024E-160-CL-12 or Phantom v7.3) captures digital holograms of the particle at frame rates between 50 and 4807.7 Hz through a 100× NA=1.4 oil-immersion objective (Nikon CFI Plan Apo VC 100X). We use HoloPy (http://manoharan.seas.harvard.edu/holopy) to fit the Lorenz-Mie scattering solution to the holograms [39]. This procedure yields the center-of-mass position of the particle to a precision better than 2 nm in all three dimensions [20] for the refractive-index-matched system.

We also look at collections of 1.9-μm-diameter sulfate polystyrene particles at an interface using bright field microscopy on a Nikon TE-2000 inverted microscope. For these experiments, we prepare sample cells with a subphase of 0.1–1% v/v particles in solutions of NaCl in water, then top the cells with decane. We omit glycerol, so that the particles sediment in the aqueous phase (ρ_{water} = 1.0 g/cm^3 and ρ_{particle} = 1.05 g/cm^3). We invert the sample cells to allow particles to sediment toward the oil-water interface for 1 h, then turn them back upright to allow particles that did not attach to the interface to sediment to the bottom of the sample cell. We then image the flat interface with a 60× water-immersion (NA=1.2) objective (Nikon CFI Plan Apo VC 60XWI).

Appendix B: Solving the Ornstein-Zernike equation under the Anisotropic Hypernetted-Chain closure

To calculate the force between the colloidal particle and the interface, we first calculate the density of ions between two flat surfaces

$$\rho(\mathbf{r}) = \rho_0 \exp\left(-\beta\left[V(\mathbf{r}) - \mu_{\mathrm{exc}}(\mathbf{r})\right]\right), \tag{B1}$$

where V is the potential energy due to the external electric field, μ_{exc} the excess chemical potential due to internal correlations, and $\beta = 1/k_{\mathrm{B}}T$. The first potential is obtained via Poisson's equation, and the second can be expressed as

$$\mu_{\mathrm{exc}}(\mathbf{r}) = \rho(\mathbf{r}) \int \mathbf{dr}'\ \frac{1}{2} h(\mathbf{r},\mathbf{r}')(h(\mathbf{r},\mathbf{r}') - c(\mathbf{r},\mathbf{r}')) - c(\mathbf{r},\mathbf{r}') \tag{B2}$$

with pair correlation functions h and c that obey the Ornstein-Zernike equation

$$h(\mathbf{r},\mathbf{r}') = c(\mathbf{r},\mathbf{r}') + \int \mathbf{dr}''\ c(\mathbf{r},\mathbf{r}'')\rho(\mathbf{r}'')h(\mathbf{r}'',\mathbf{r}') \tag{B3}$$

using the so-called Hyper-Netted Chain approximation

$$c(\mathbf{r},\mathbf{r}') = h(\mathbf{r},\mathbf{r}') - \ln(1 + h(\mathbf{r},\mathbf{r}')) - \beta u(\mathbf{r},\mathbf{r}'), \tag{B4}$$

where u is the pair potential. These equations form a complete set, and in addition to the ion profiles, yield information about the pair correlation functions—that is, the local structure within the ion cloud. Equations (B2)-(B4) become numerically tractable in the geometry in this work, which reduces μ_{exc} and ρ to functions of a single coordinate z along the axis perpendicular to the boundaries (interface and particle), and the pair correlation functions to functions of three coordinates z, z', and r, where r is a cylindrical coordinate perpendicular to the z-axis. This method has been pioneered and extensively applied by Kjellander, Marčelja *et al.* (for example in Reference [40]). From the ion profiles we obtain the disjoining pressure

$$P_{zz}(d) = -\int_0^d \mathrm{d}z\ \rho(z)\frac{\partial U}{\partial z}, \tag{B5}$$

where U is the interaction between the ions and the boundaries (which is electrostatic and steric), and d is the separation between the boundaries. Given that the typical correlation length (approximately 1 nm) is three orders of magnitude smaller than the radius of the colloidal particle (approximately 1 μm), the Derjaguin approximation can be used to obtain an accurate value for

the force F between a sphere and a flat surface

$$F(d) = -2\pi R \int_d^\infty \mathrm{d}q \; P_{zz}(q), \tag{B6}$$

with R the particle radius. The integration of F finally leads to the effective pair potential between the sphere and the boundary. We use a value of -50mV for the zeta potential of the sphere. The specific value of the zeta potential, however, has a small effect on the predicted salt concentration regimes where different binding modes are expected. This can be understood from the underlying mechanism, the structural reordering of the ion cloud, which follows from a competition between steric and electrostatic effects. Excluded volume effects depend on the packing fraction and become significant for concentrations around 0.2–0.4 M (for ions with a hydrated radius of 0.35 nm), such that structural reorganization is found to occur in that regime, regardless of the magnitude of the surface potential [41].

Appendix C: Additional experimental observations

1. Binding and unbinding of particles

In addition to seeing particles transition from being bound without breaching to breaching the interface, we also find that some particles can bind to an interface, unbind, then bind again (as shown in Fig. 9). Further evidence for this time-varying interaction comes from experiments on silica particles. Owing to their density, we can tell whether a silica particle is bound to the interface by looking at the trajectory upon approach from the aqueous phase. Fig. 10 shows the trajectory of a 1-μm-diameter aminopropyltrimethoxysilane-functionalized silica particle that we push toward a water-decane interface with radiation pressure, against gravity. The fluctuations in z show that the particle binds to the water-decane interface at 2.5 s, falls off at 6 s, then binds again at 11 s, where it remains for the rest of the observation window.

When the silica particle binds to the interface, it is unlikely that it has breached it. At even a small equilibrium contact angle ($\theta_E = 5°$), a 1-μm particle that breaches the interface requires a 100 k_BT fluctuation to detach, given the oil-water interfacial tension. Therefore detachment is unlikely to occur on timescales of seconds for even very small contact angles. A more likely explanation for the time-dependent binding is that the particle is bound but not breached, falls off, and reattaches again. Such behavior is consistent with our hypothesis that the rotational diffusion of particles can present patches of varying charge density to the interface, resulting in time-varying normal interactions.

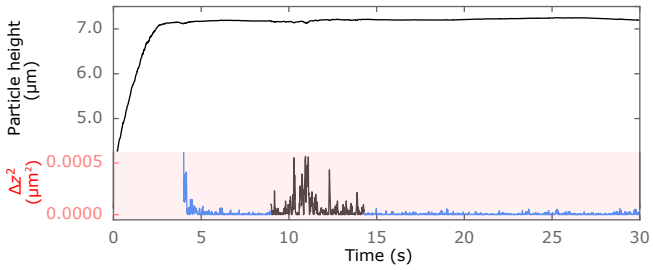

FIG. 9. Time-dependent binding of a polystyrene particle to an interface. Trajectory of a 1.9-μm-diameter sulfate polystyrene particle that is pushed to an interface between glycerol/water and decane with radiation pressure. The particle binds to the interface at 5 s, unbinds at 9 s, and binds again at 14 s. Data was taken at 100 Hz.

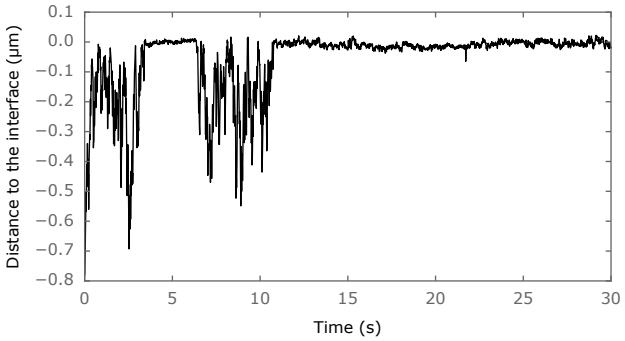

FIG. 10. Time-dependent binding of a 1-μm-diameter APTMS-silica particle to an interface. Trajectory of an APTMS-silica particle that is pushed to a water-decane interface with radiation pressure. The particle binds to the interface at 2.5 s, falls off at 6 s, then is pushed back to the interface and re-binds at 11 s. Data was taken at 100 Hz.

2. Particles binding to water-decane interfaces

As we describe in the main text, we prepare samples without glycerol in the aqueous phase and look at large numbers of particles at the interface. In this aqueous solution, the polystyrene particles sediment away from the interface when the sample cell is upright. Any particles that are bound to the interface are therefore held there by an attractive force.

The refractive-index mismatch between the aqueous and oil phases allows us to distinguish particles that have bound after breaching the high-index decane phase from ones that are bound but are still fully submerged in the aqueous phase.

We see that at high salt concentrations, the particles form a repulsive crystal, but the interface is much less ordered at lower salt concentrations (Fig. 11). The fraction of particles that bind to the interface also increases with salt concentration.

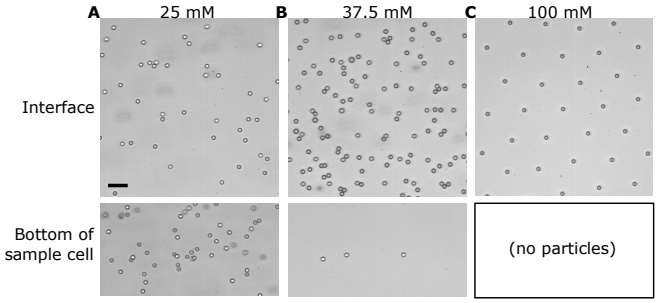

FIG. 11. Normal interactions depend on salt concentration. We prepare sample cells with either (A) 25 mM, (B) 37.5 mM, or (C) 100 mM NaCl in the water phase. The unbound particles that settle to the bottom of the sample are shown in the bottom images. The scale bar is 10 μm.

Appendix D: DLVO calculations and Boltzmann inversion

1. DLVO calculations

In the main text, we note that DLVO theory does not explain the binding that we observe. We calculate the potential between the particle and interface using a model that accounts for the electrostatic repulsion from the interface and the van der Waals attraction. We also use the measured value (see Materials and Methods) of the zeta potential for the particle in 100 mM NaCl glycerol/water solution, ζ_s = -55 mV. We find that even for a conservatively small value for the zeta potential of the interface, ζ_p = -10 mV, the predicted potential is always repulsive at at distances more than 1 nm from the interface, suggesting that the attraction between the particle and interface is underestimated by DLVO. Below, we give the details of our calculation.

We describe the interaction potential $W_{\rm tot}$ between a negatively charged particle and the interface in our system using classical DLVO theory, taking into account the van der Waals and electric double-layer interaction between the particle and the interface, and the interaction between a particle and its image charge:

$$W_{\rm tot} = W_{\rm vdW} + W_{\rm image} + W_{\rm interface}. \tag{D1}$$

Below, we describe how we calculate each of the terms in the above equation.

a. *van der Waals interaction*

To calculate the van der Waals interaction $W_{\rm vdW}$, we first calculate the Hamaker constant for polystyrene particle and decane interacting through a glycerol/water aqueous phase that is refractive index-matched to decane. We use the Lifshitz approximation:

$$A = \frac{3kT}{4}\frac{\epsilon_{\rm PS}-\epsilon_{\rm aq}}{\epsilon_{\rm PS}+\epsilon_{\rm aq}}\frac{\epsilon_{\rm decane}-\epsilon_{\rm aq}}{\epsilon_{\rm decane}+\epsilon_{\rm aq}}, \tag{D2}$$

where $\epsilon_{\rm PS}$ = 2.6, $\epsilon_{\rm aq}$ = 62 for the glycerol/water system [42], and $\epsilon_{\rm decane}$ = 2. The dispersion contribution is zero because the interface is refractive-index matched [29].

We then use the Derjaguin approximation to calculate the van der Waals interaction between a sphere and a flat surface separated by a distance D, taking into account the screening of the nonretarded Hamaker constant in an electrolyte:

$$W(D)_{\rm vdW} = -\frac{AR}{6D}e^{-\kappa D}, \tag{D3}$$

where for a given monovalent salt concentration C, $\kappa^{-1} = q^{-1}\sqrt{\epsilon_{\rm aq}\epsilon_0 kT/2C}$ is the inverse of the Debye length, q is the elementary charge, and ϵ_0 is the permittivity of free space.

b. *Image charge*

The image charge q' of a charge q in a glycerol/water phase ($\epsilon_{\rm aq}$) near a planar boundary with decane ($\epsilon_{\rm decane}$) is given by

$$q' = q\frac{\epsilon_{\rm aq}-\epsilon_{\rm decane}}{\epsilon_{\rm aq}+\epsilon_{\rm decane}} \simeq 0.94q. \tag{D4}$$

For a sphere with zeta potential ζ_s, we therefore use the approximation that the potential of its image is also ζ_s.

We use the Sader, Carnie, and Chan [43] formulation for the double-layer interaction between two spheres to calculate the potential arising from a charged sphere interacting with its image. This model is an extension of the Hogg, Healy, and Fuerstenau solution [44] for validity at all κD, and potentials up to ±100 mV:

$$W_{\rm image} = \epsilon_{\rm aq}\epsilon_0\left(\frac{Y_D kT}{q}\right)^2\frac{R^2}{2(R+D)}\ln(1+e^{-2\kappa D}). \tag{D5}$$

Here $Y_D = 4e^{\kappa D}\tanh^{-1}(e^{-\kappa D}\tanh(y_s/4))$, and $y_s = q\zeta_s/kT$ is the reduced surface potential for the sphere.

Although our particles interact with their image across an interface, and the Sader, Carnie, and Chan formulation is intended for two charged spheres interacting in a homogeneous medium, it is the best approximation we know of for our system. There is a model for particles that interact with their image across an interface [45], but this model applies to particles in oil, and there is no clear avenue to adapt it for our system.

c. *Interface term*

We also calculate the potential between a sphere and a plane using the Sader, Carnie, and Chan formulation [43]

for two spheres of different surface potentials in the limit where the the second sphere has an infinite radius:

$$W_{\text{interface}} = \epsilon_{\text{aq}}\epsilon_0 R \left(\frac{kT}{2q}\right)^2 \times \left((y_s + y_p)^2 \ln(1 + e^{-\kappa D}) + (y_s - y_p)^2 \ln(1 - e^{-\kappa D})\right), \tag{D6}$$

where $y_s = q\zeta_p/kT$ is the reduced surface potential for the plane.

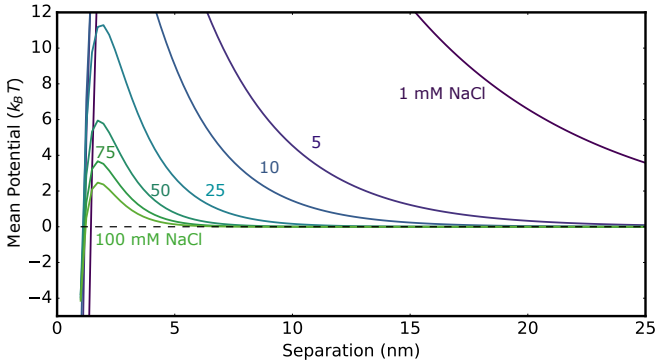

FIG. 12. DLVO theory, modified to include effects of the interface, does not explain the observed interactions. Plot shows the mean potentials between a polystyrene particle and an interface with glycerol/water on one side and decane on the other as a function of salt concentration with zeta potential ζ_{p} = -10 mV for the plane and ζ_{s} = -55 mV for the particle.

We use ζ_{p} = -10 mV and ζ_{s} = -55 mV to generate potentials with a conservatively small electrostatic repulsion component, and yet this model still predicts purely repulsive behavior for the particle at distances greater than 1 nm from the interface, as shown in Fig. 12.

The theory does predict a secondary minimum in the interaction potential for some combinations of salt concentrations, though only for particles and interfaces with much lower zeta potentials and not for the salt concentrations we observe. Variations on DLVO theory—including both numerical and analytical versions, and boundary conditions including constant charge, constant potential, and charge regulation—also fail to reproduce our results. The quantitative differences between our data and theoretical calculations are not surprising, given the limited range of applicability for DLVO.

2. Boltzmann inversion

To determine the potential between bound particles from the measured fluctuations, we use the Boltzmann distribution. In equilibrium, the probability of finding a particle at position z given a potential well $U(z)$ is

$$P(z) = \frac{1}{Z}\exp\left(-\frac{U(z)}{kT}\right), \tag{D7}$$

where Z is the partition function. To minimize the effect of drift from the microscope stage, the sample, or—in the case of particles that have breached the interface—their logarithmic relaxation, we calculate the displacement of the particles from a mean position at a given time t. This mean $\overline{z(t)}$ is a centered sliding average of the height over a chosen time interval. Here we choose a time window of 1 s unless the mode of binding is much shorter-lived than a few seconds, in which case we choose a window of 0.2 s. The displacements are thus $z = z_m(t) - \overline{z(t)}$, where $z_m(t)$ is the measured height of the particle from holography.

We bin the measured displacements in z to determine $P(z)$, then invert the distribution to find the potential well $U(z)$:

$$U(z) = -kT(\ln P(z) + \ln Z) = -kT \ln P(z) + C. \tag{D8}$$

Because our trajectories are usually a few thousand frames in length, the lowest non-zero probability we can measure for a bin is order 1/1000. Therefore, from equation D8, the maximum measurable potential is approximately 7 kT above the minimum of the well.

To extract the binding stiffness from the inversions, we assume a harmonic potential with binding stiffness K and an additive constant C. Because $\ln Z$ is also an additive constant, we write

$$U(z) = \frac{1}{2}Kz^2 + C. \tag{D9}$$

We use a least-squares method to find K and C in Equation D9 for the measured $P(z)$. The best-fit K is what we report for the binding stiffness in the main text.

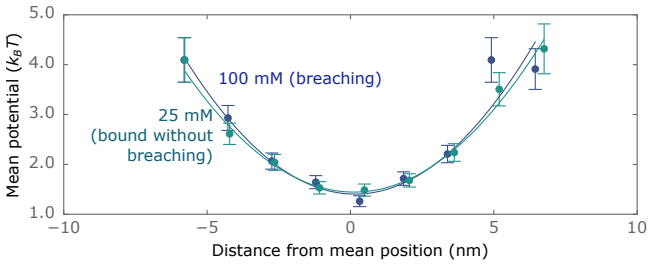

FIG. 13. Inverting the distribution of the fluctuations of the particles from their mean position (over 1 s) reveals how the particles are confined. Negative values indicate a position closer to the interface. The error bars are the square root of the number of values in each of the bins scaled by kT, and the solid lines are fits to a harmonic potential.

As expected, we find that particles bound to the interface at 100 mM NaCl appear to be confined in a well with width limited by the noise of our measurement technique (approximately 2 nm in the axial direction at 1 kT). Using equation D9, we find that noise limits the stiffest binding we can measure to 0.8 mN/m for a sliding average window of 1 s, and 1.7 mN/m for a sliding average over 0.2 s.

Because the particles that are bound without breaching show confinement similar to that of the breaching particles (Fig. 13), we estimate that the particles are bound to the interface with a stiffness of at least 1 mN/m.

Appendix E: Movie 1

Real-time holographic movie of a particle that is bound but not breached (left) and a particle that is breached (right) interacting. The inset shows reconstructions of the holograms, mimicking a bright-field image.

[1] Bernard P. Binks and Tommy S. Horozov, *Colloidal Particles at Liquid Interfaces* (Cambridge University Press, Cambridge, 2006).

[2] Robert Aveyard, Bernard P. Binks, and John H. Clint, "Emulsions stabilised solely by colloidal particles," Advances in Colloid and Interface Science **100-102**, 503–546 (2003).

[3] A. D. Dinsmore, Ming F. Hsu, M. G. Nikolaides, Manuel Marquez, A. R. Bausch, and D. A. Weitz, "Colloidosomes: Selectively Permeable Capsules Composed of Colloidal Particles," Science **298**, 1006–1009 (2002).

[4] Ming Pan, Fengjiao Lyu, and Sindy K. Y. Tang, "Fluorinated Pickering Emulsions with Nonadsorbing Interfaces for Droplet-based Enzymatic Assays," Analytical Chemistry **87**, 7938–7943 (2015).

[5] E. M. Herzig, K. A. White, A. B. Schofield, W. C. K. Poon, and P. S. Clegg, "Bicontinuous emulsions stabilized solely by colloidal particles," Nature Materials **6**, 966–971 (2007).

[6] R. McGorty, J. Fung, D. Kaz, and V. N Manoharan, "Colloidal self-assembly at an interface," Materials Today **13**, 34–42 (2010).

[7] Pawel Pieranski, "Two-dimensional interfacial colloidal crystals," Physical Review Letters **45**, 569–572 (1980).

[8] K. Zahn and G. Maret, "Dynamic criteria for melting in two dimensions," Physical Review Letters **85**, 3656–3659 (2000).

[9] Peter Lipowsky, Mark J. Bowick, Jan H. Meinke, David R. Nelson, and Andreas R. Bausch, "Direct visualization of dislocation dynamics in grain-boundary scars," Nature Materials **4**, 407–411 (2005).

[10] R. Aveyard, B. P. Binks, J. H. Clint, P. D. I. Fletcher, T. S. Horozov, B. Neumann, V. N. Paunov, J. Annesley, S. W. Botchway, D. Nees, A. W. Parker, A. D. Ward, and A. N. Burgess, "Measurement of long-range repulsive forces between charged particles at an oil-water interface," Physical Review Letters **88**, 246102–246105 (2002).

[11] M. G. Nikolaides, A. R. Bausch, M. F. Hsu, A. D. Dinsmore, M. P. Brenner, C. Gay, and D. A. Weitz, "Electric-field-induced capillary attraction between like-charged particles at liquid interfaces," Nature **420**, 299–301 (2002).

[12] Bum Jun Park and Eric M. Furst, "Attractive interactions between colloids at the oil-water interface," Soft Matter **7**, 7676–7682 (2011).

[13] Wei Chen, Susheng Tan, Yi Zhou, Tai-Kai Ng, Warren T. Ford, and Penger Tong, "Attraction between weakly charged silica spheres at a water-air interface induced by surface-charge heterogeneity," Physical Review E **79**, 041403 (2009).

[14] Bum Jun Park, Jan Vermant, and Eric M. Furst, "Heterogeneity of the electrostatic repulsion between colloids at the oil-water interface," Soft Matter **6**, 5327–5333 (2010).

[15] Mina Lee, Daeyeon Lee, and Bum Jun Park, "Effect of interaction heterogeneity on colloidal arrangements at a curved oil-water interface," Soft Matter **11**, 318–323 (2015).

[16] F. Bresme and M. Oettel, "Nanoparticles at fluid interfaces," Journal of Physics: Condensed Matter **19**, 413101 (2007).

[17] Kasper Masschaele, Bum Jun Park, Eric M. Furst, Jan Fransaer, and Jan Vermant, "Finite ion-size effects dominate the interaction between charged colloidal particles at an oil-water interface," Phys. Rev. Lett. **105**, 048303 (2010).

[18] Sebastian Uppapalli and Hui Zhao, "The influence of particle size and residual charge on electrostatic interactions between charged colloidal particles at an oil-water interface," Soft Matter **10**, 4555–4560 (2014).

[19] Dimitris Stamou, Claus Duschl, and Diethelm Johannsmann, "Long-range attraction between colloidal spheres at the air-water interface: The consequence of an irregular meniscus," Physical Review E **62**, 5263 (2000).

[20] David M. Kaz, Ryan McGorty, Madhav Mani, Michael P. Brenner, and Vinothan N. Manoharan, "Physical ageing of the contact line on colloidal particles at liquid interfaces," Nature Materials **11**, 138–142 (2012).

[21] Anna Wang, Ryan McGorty, David M. Kaz, and Vinothan N. Manoharan, "Contact-line pinning controls how quickly colloidal particles equilibrate with liquid interfaces," Soft Matter **12**, 8958–8967 (2016).

[22] Howard Brenner, "The slow motion of a sphere through a viscous fluid towards a plane surface," Chemical Engineering Science **16**, 242–251 (1961).

[23] H. Jensenius and G. Zocchi, "Measuring the spring constant of a single polymer chain," Phys. Rev. Lett. **79**, 5030–5033 (1997).

[24] Francisco J. Solis and Monica Olvera de la Cruz, "Collapse of flexible polyelectrolytes in multivalent salt solutions," The Journal of Chemical Physics **112**, 2030–2035 (2000).

[25] Pai-Yi Hsiao and Erik Luijten, "Salt-induced collapse and reexpansion of highly charged flexible polyelectrolytes," Phys. Rev. Lett. **97**, 148301 (2006).

[26] M. E Leunissen, A. Van Blaaderen, A. D Hollingsworth, M. T Sullivan, and P. M Chaikin, "Electrostatics at the oil-water interface, stability, and order in emulsions and colloids," Proceedings of the National Academy of Sciences **104**, 2585–2590 (2007).

[27] Colm P Kelleher, Anna Wang, Guillermo Iván Guerrero-García, Andrew D Hollingsworth, Rodrigo E Guerra, Bhaskar Jyoti Krishnatreya, David G Grier, Vinothan N Manoharan, and Paul M Chaikin, "Charged hydrophobic colloids at an oil–aqueous phase interface," Physical

Review E **92**, 062306 (2015).
[28] Nina A. Elbers, Jessi E. S. van der Hoeven, D. A. Matthijs de Winter, Chris T. W. M. Schneijdenberg, Marjolein N. van der Linden, Laura Filion, and Alfons van Blaaderen, "Repulsive van der Waals forces enable Pickering emulsions with non-touching colloids," Soft Matter **12**, 7265–7272 (2016).
[29] Jacob N. Israelachvili, *Intermolecular and Surface Forces*, 3rd ed. (Elsevier, Amsterdam, 2011).
[30] Laurent Helden, Kilian Dietrich, and Clemens Bechinger, "Interactions of colloidal particles and droplets with wateroil interfaces measured by total internal reflection microscopy," Langmuir **32**, 13752–13758 (2016).
[31] Jos W. Zwanikken and Monica Olvera de la Cruz, "Tunable soft structure in charged fluids confined by dielectric interfaces," Proceedings of the National Academy of Sciences **110**, 5301–5308 (2013).
[32] Roland Kjellander and Stjepan Marčelja, "Correlation and image charge effects in electric double layers," Chemical Physics Letters **112**, 49 – 53 (1984).
[33] Yufei Jing, Vikram Jadhao, Jos W. Zwanikken, and Monica Olvera de la Cruz, "Ionic structure in liquids confined by dielectric interfaces," The Journal of Chemical Physics **143**, 194508 (2015).
[34] Dong Woo Kang, Jin Hyun Lim, and Bum Jun Park, "Heterogeneous interface adsorption of colloidal particles," Soft Matter **13**, 6234–6242 (2017).
[35] "Calculate density and viscosity of glycerol/water mixtures," `http://www.met.reading.ac.uk/~sws04cdw/viscosity_calc.html`, accessed: 2018-01-13.
[36] Grant B. Webber, Rogerio Manica, Scott A. Edwards, Steven L. Carnie, Geoffrey W. Stevens, Franz Grieser, Raymond R. Dagastine, and Chan, "Dynamic forces between a moving particle and a deformable drop," J. Phys. Chem. C **112**, 567–574 (2007).
[37] Hongzhi Wang, Virendra Singh, and Sven Holger Behrens, "Image charge effects on the formation of Pickering emulsions," The Journal of Physical Chemistry Letters **3**, 2986–2990 (2012).
[38] Bronislaw Jańczuk, Wieslaw Wójcik, and Anna Zdziennicka, "Determination of the components of the surface tension of some liquids from interfacial liquid-liquid tension measurements," Journal of Colloid and Interface Science **157**, 384 – 393 (1993).
[39] Sang-Hyuk Lee, Yohai Roichman, Ga-Ra Yi, Shin-Hyun Kim, Yang Seung-Man, Alfons van Blaaderen, Peter van Oostrum, and David G. Grier, "Characterizing and tracking single colloidal particles with video holographic microscopy," Optics Express **15**, 18275–18282 (2007).
[40] R Kjellander, T Åkesson, Bo Jönsson, and S Marcelja, "Double layer interactions in mono-and divalent electrolytes: a comparison of the anisotropic hypernetted chain theory and Monte Carlo simulations," The Journal of chemical physics **97**, 1424–1431 (1992).
[41] José Guadalupe Ibarra-Armenta, Alberto Martín-Molina, and Manuel Quesada-Pérez, "Influence of monovalent ion size on colloidal forces probed by Monte Carlo simulations," Physical Chemistry Chemical Physics **13**, 13349–13357 (2011).
[42] D.L. Sorby, R.G. Bitter, and J.G. Webb, "Dielectric constants of complex pharmaceutical solvent systems I: Water-ethanol-glycerin and water-ethanol-propylene glycol," Journal of Pharmaceutical Sciences **52**, 1149 – 1153 (1963).
[43] John E. Sader, Steven L. Carnie, and Derek Y. C. Chan, "Accurate analytic formulas for double-layer interaction between spheres," Journal of Colloid and Interface Science **171**, 46–54 (1995).
[44] R. Hogg, T. W. Healy, and D. W. Fuerstenau, "Mutual coagulation of colloidal dispersions," Trans. Faraday Soc. **62**, 1638–1651 (1966).
[45] K. D. Danov, P. A. Kralchevsky, K. P. Ananthapadmanabhan, and A. Lips, "Particle-interface interaction across a nonpolar medium in relation to the production of particle-stabilized emulsions," Langmuir **22**, 106–115 (2006).